SUMMERTIME ATMOSPHERIC CIRCULATION IN THE VICINITY OF A BLUE ICE AREA IN QUEEN MAUD LAND, ANTARCTICA

MICHIEL R. VAN DEN BROEKE and RICHARD BINTANJA
Institute for Marine and Atmospheric Research Utrecht, Utrecht University, Princetonplein 5, 3584 CC Utrecht, The Netherlands, e-mail:broeke@fys.ruu.nl

(Received in final form 9 August, 1994)

Abstract. The surface wind field is an important factor controlling the surface mass balance of Antarctica. This paper focuses on the observed atmospheric circulation during summer of an Antarctic blue ice area in Queen Maud Land. Blue ice areas are characterised by a negative surface mass balance and henceforth provide an interesting location to study the influence of meteorological processes on large local mass balance gradients. During lapse conditions, synoptic forcing determines the surface-layer flow. No significant horizontal temperature gradient with coastal stations could be detected along isobaric surfaces, indicating weak or absent thermal wind. Observations performed at the coastal stations Halley and Georg von Neumayer show the pronounced effects of synoptic forcing. The surface winds in the valley of the blue ice area could be divided into two distinct flow patterns, occurring with about equal frequency during the experiment. Flow type I is associated with cyclonic activity at the coast, resulting in strong easterly winds, precipitation and drifting snow. Flow characteristics inside and outside of the valley are similar during these conditions. Flow type II occurs when a high pressure system develops in the Weddell Sea, weakening the free atmosphere geostrophic winds. A local circulation is able to develop inside the valley of the blue ice area during these tranquil conditions. The transition from flow type II to flow type I is associated with front-like phenomena inside the valley. Some simple theoretical considerations show that surface-layer stability and the upper air geostrophic wind determine the surface flow direction in the valley. Finally, the influence of the observed circulation on the energy and mass balance of the blue ice area is discussed.

1. Introduction

Although Antarctica is generally regarded as one large accumulation area, the surface mass balance is negative in blue ice areas (BIA's) (Fujii and Kusunoki, 1982; Jonsson, 1992). These areas only cover a minor part of the Antarctic ice sheet, but their occurrence raises many questions. Orheim and Lucchitta (1990) proposed to use BIA size as an indicator for a changing Antarctic climate: an increase in precipitation would consequently lead to a decrease of BIA extent. A possible formation mechanism for BIA's is schematically drawn in Figure 1. In general, the katabatic winds over the Antarctic ice sheet increase towards the coast, and become more directed down the fall line of the topography. This induces a divergence of drifting snow transport that serves as a negative term in the surface mass balance (erosion). This term is normally small, compared to the amount of precipitation. If a nunatak (a mountain range that penetrates through the ice) obstructs the surface-bounded snow drift, the lee side of the mountain will experience increased erosion: the mass removed from the surface by the wind is only partly replaced from the upstream area. When erosion plus evaporation (which is usually small) exceeds the amount of precipitated snow, the local mass balance becomes negative. The net removal of snow and firn will finally result in the surfacing of glacier ice with a

Boundary-Layer Meteorology **72:** 411–438, 1995.

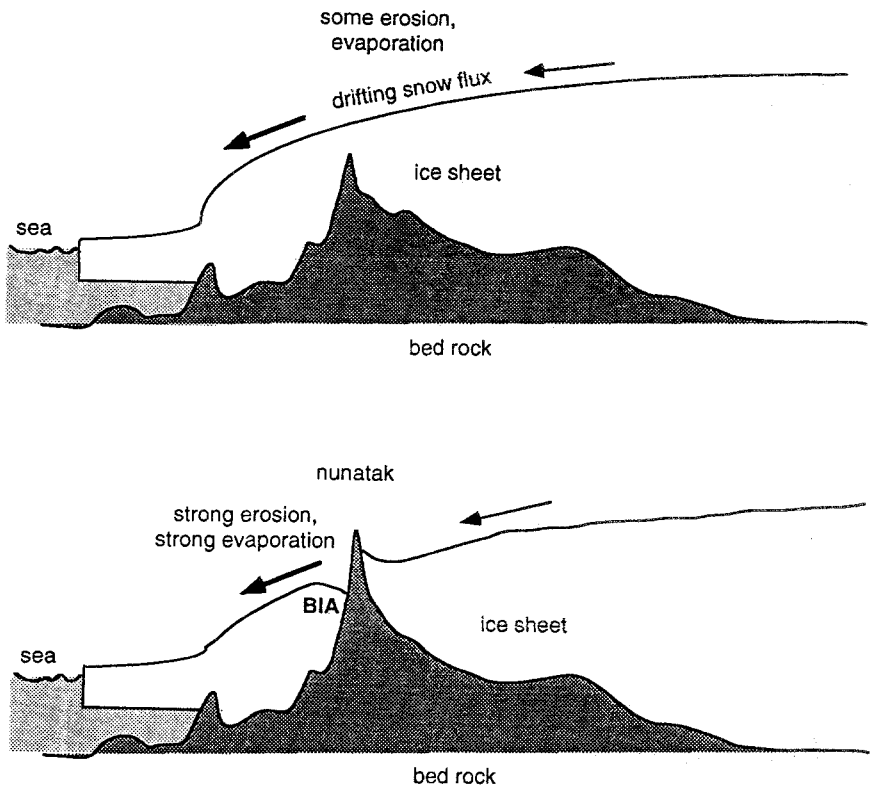

Fig. 1. Schematic representation of a possible BIA formation mechanism. Upper panel: undisturbed snow drift transport. Erosion is caused by large-scale divergence of the katabatic wind. Where a nunatak penetrates the ice sheet (lower panel), removal of snow at the lee side is not resupplied from the upstream area owing to the shielding effect of the nunatak. The surface will start to erode, until glacier ice (blue ice) surfaces. The low albedo of blue ice promotes evaporation.

milky blue appearance, often called "blue ice". Takahashi *et al.* (1988) calculated large-scale drifting snow divergence over Mizuho plateau, where no nunataks are present to obstruct drifting snow, to explain the existence of BIA's. BIA's at higher elevations (2000 m and up) have received much attention as meteorite traps (Cassidy *et al.*, 1992).

Once formed, BIA's tend to persist. For instance, new snow, deposited on the blue ice either by drifting or precipitation, can hardly settle on the smooth surface. The low surface albedo of blue ice, compared to its snowy surroundings, promotes evaporation of the ice surface, further enhancing the horizontal mass balance gradient. Since the amount of precipitation increases sharply when descending towards the coast (Fortuin and Oerlemans, 1990) and the winds in the interior of the continent are much more gentle (Wendler and Kodama, 1985; Parish and Bromwich, 1991), the most likely region for BIA's to occur is the intermediate plateau, where strong winds and relatively low accumulation rates prevail.

From all points of view, it appears that the surface wind field plays a crucial role in the formation and maintenance of BIA's. A meteorological/glaciological experiment, hosted by SWEDARP 92-93 (Swedish Antarctic Research Programme) was initiated in order to map the climate of a representative BIA. As a first step towards understanding the dynamics of BIA formation, this paper describes the forcing of the surface winds as observed close to and over a representative BIA. The interaction with the surface energy- and mass balance is discussed. A more detailed description of the energy balance is presented in Bintanja and Van den Broeke (in press). Continental scale interaction of katabatic wind and BIA formation is the subject of a third paper on this subject (Van den Broeke and Bintanja, in press).

2. Location of the Experiment and Set-Up

Scharffenbergbotnen (from now on SBB) is a small valley (2×5 km^2) located in the Heimefrontfjella, a mountain range in Western Queen Maud Land (Figure 2). The Heimefrontfjella is directed NE–SW while the mountains that surround SBB are oriented perpendicular to this direction. The Heimefrontfjella marks a sudden transition from the coastal area to the high plateau. The blocking of the ice flow results in a large altitude gradient from 1200 m a.s.l. inside the valley to over 2500 m a.s.l. at the Amundsenisen plateau. Net accumulation rates outside the valley are approximately 20 cm w.e. yr^{-1}, while inside the valley a net sublimation rate of 20 cm w.e. yr^{-1} has been measured (Jonsson, 1992), both numbers showing large interannual variations. In the bottom of the valley, the ablation rates are highest: 1 mm per day during the summer. During the present experiment, melting did not occur. Halfway along the valley a snow ridge has formed that extends across the depression.

During the present experiment, seven masts were installed in and outside SBB; (Figure 2). Each mast measured wind speed and temperature at 2 and 6 m and wind direction at 6 m, while at sites 2 and 3, measurements were also taken at 0.5 m. The total radiation budget was measured at sites 2 and 3, while upward and downward short-wave radiation fluxes were measured at sites 1, 2, 3, 5 and 7. Humidity was measured at three levels at sites 2 and 3 and at two levels at site 7. Data were sent to the base camp by radio telemetry. The masts at sites 2 to 7 were checked regularly for icing and leaning. Near Svea (site 7) every 6 h a cabled, helium-filled balloon sampled the lowest 800 to 1500 m of the atmosphere, measuring pressure, temperature, humidity, wind speed and wind direction. All data collected by the balloon were converted to average values over 10 m increments, using the hydrostatic approximation and a least squares fit in 40 m intervals. During 9 days of fine weather, the sounding frequency was intensified to once every 3 h. The balloon system can not be operated if surface wind speed exceeds 10 m s^{-1}. More detailed information about the experiment can be found in Bintanja *et al.* (1993). This experimental set-up has been used successfully on glaciers in the Alps, at

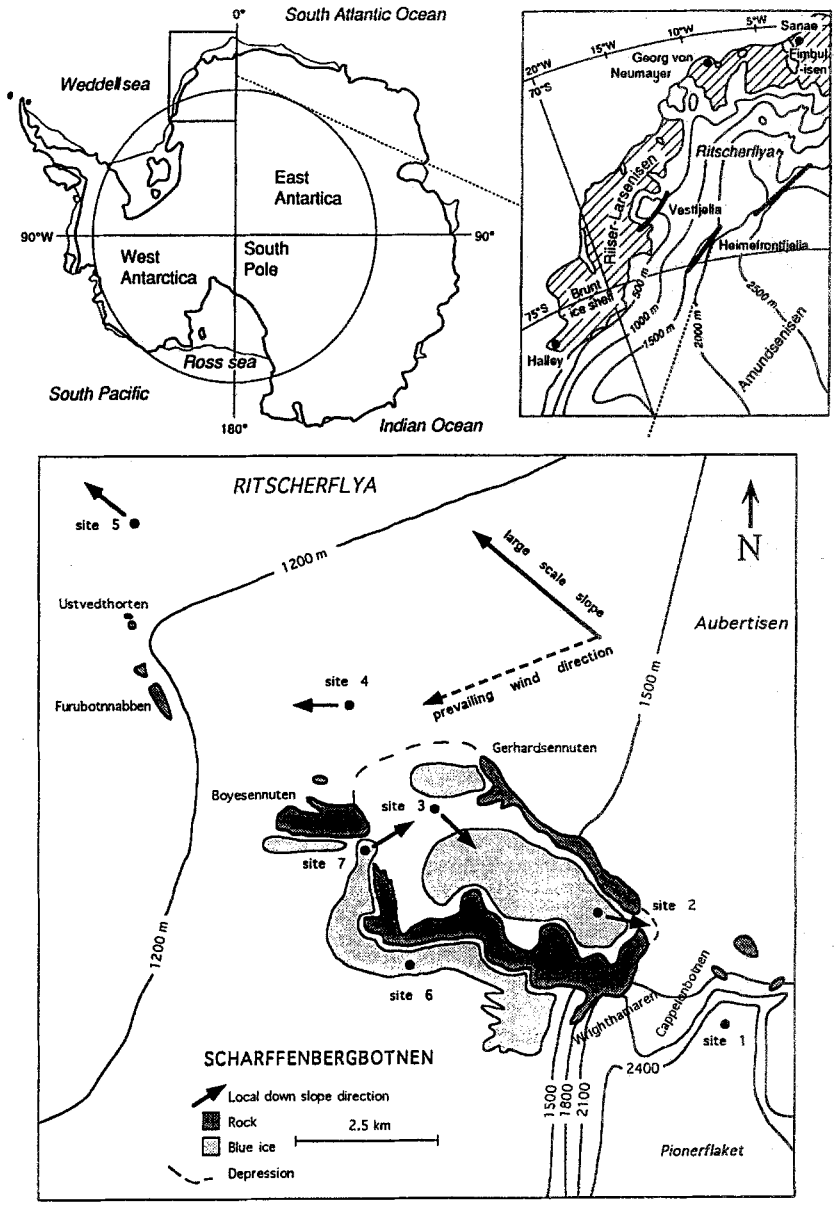

Fig. 2. Location and set-up of the experiment.

King George Island and in the ablation zone of the Greenland ice sheet (Oerlemans and Vugts, 1993).

In recent years, investigations in SBB have been performed by Jonsson (1992) during the SWEDARP expeditions from 1988 to 1992. In order to study the local climate of SBB, he used two automatic weather stations. One was situated in the bottom of the valley on the blue ice and the other 12 km to the NW outside the

TABLE I

Availability of mast data and number of balloon soundings used in this analysis during the period 31 December 1992–10 February 1993

Site no.	Masts		Balloon	
	Surface type	Performance	Time (UT)	Total number
2	Blue ice	93%	00 UT	9
			03 UT	13
3	Snow	100%	06 UT	9
			09 UT	16
4	Snow	100%	12 UT	10
			15 UT	14
5	Snow	76%	18 UT	11
			21 UT	13
7	Blue ice	100%		
			Halley (12 UT)	31
			GvN (10 UT)	28

valley. He found that the wind inside the valley was more gusty and had a smaller directional constancy (0.95 vs. 0.85) than outside the valley during the period considered (18 January–18 February 1988). Mean wind speed was the same for both stations, 4 m s^{-1}, which is a remarkably low value for the escarpment area even in summer, compared for instance with 11 m s^{-1} in Adelie land (1560 m a.s.l.), as observed by Kodama *et al.* (1989). During calm periods throughout the year, the formation of a pool of cold, stagnant air was observed inside the depression. Removal of this cold air occurred suddenly by entrainment of the large-scale flow into the valley.

The data set used in this paper covers the period 31 December 1992 to 10 February 1993, a total of 42 days. Table I lists the availability of data at the different sites and the number of balloon soundings performed at Svea and two coastal stations. Data of these stations, Halley (75°35′ S, 26°50′ W) and Georg von Neumayer (GvN, 70°37′ S, 8°22′ W), were provided by the British Antarctic Survey. Data from sites 1 and 6 will not be used in the present analysis. The mast at site 5 did not work continuously until after the third week, resulting in a 24% data loss. However, this mast produced valuable information concerning the wind climate outside SBB, as will be discussed in Section 5.

The mast at site 5 was presumed to measure the undisturbed conditions while the other masts experienced more or less the influence of the topography and the blue ice of SBB. Arrows in Figure 2 indicate the direction of the local topographic fall line at each site. Since the valley forms a depression, the local fall lines show a high diversity of values at the different sites. Down-slope direction of the continental

TABLE II

Surface roughness (taken from Bintanja and Van den Broeke, in press)

	Site 2	Site 3	Site 4	Site 5
z_0 (mm)	0.007	0.084	0.55	0.75

slope in the area is estimated to be 130 deg (approximately SW–NW) with a slope magnitude of 17 m km^{-1}. Note that only at site 5 does the local fall line coincide with this large-scale fall line. Not only the slope direction and magnitude, but also the aerodynamic surface roughness shows a large variety from place to place. Table II lists the values (taken from Bintanja and Van den Broeke, in press). The aerodynamic roughness of the snow surface increases farther away from the valley, owing to the larger sastrugi elements. The value of z_0 over the blue ice of 0.007 mm is probably the lowest value of any permanent natural surface on earth.

3. General Atmospheric Circulation over Antarctica

Next we shall discuss three important forcing mechanisms that generally determine boundary-layer air flow in the Antarctic. A mesoscale effect is introduced by cooling of the air overlying the continent. Lifting of the isentropic surfaces (Kottmeier and Stuckenberg, 1986) introduces baroclinity in the coastal area. The associated thermal wind relation is:

$$u_{T//} = \frac{\partial u_g}{\partial z} = -\frac{g}{fT}\left(\frac{\partial T}{\partial y}\right)_p, \tag{1}$$

where // means parallel to the contours of the terrain, u_g is the geostrophic wind parallel to the contour lines and the temperature gradient $\partial T/\partial y$ is taken perpendicular to the coast and along lines of constant pressure. The mean thermal field induces an east-west directed surface geostrophic wind over the continent, which is largest in the coastal areas, as suggested by Kottmeier and Stuckenberg (1986), since the slope of the isentropic surface is largest there.

Close to the surface, the strong cooling of the air introduces a sloped-inversion pressure gradient that forces the notorious Antarctic katabatic winds. These katabatic winds are a semi-permanent feature during the winter months but are weaker in summer, when the surface inversion is weak or destroyed. Katabatic surges in the Antarctic coastal area exhibit extreme strength and persistance, as discussed by many authors (Ball, 1956; Parish, 1984; Bromwich, 1989; Pettré and André, 1991). The inversion winds on the high Antarctic plateau, where slope angles are gentle, are weaker and directed more across the slope under the influence of the Coriolis

force (Mahrt and Schwerdtfeger, 1970; Parish and Waight, 1987). However, they still show remarkable directional constancy. Some data are available covering the intermediate region between the interior and the coast (Ohata *et al.*, 1985; Kodama *et al.*, 1989; Sorbjan *et al.*, 1986; Wendler and Kodama, 1985). The climate of the dry valleys was investigated by McKendry and Lewthwaite (1989) and Clow *et al.* (1988).

The third effect influencing the surface flow pattern, especially in the coastal areas, is the belt of minimum surface pressure at approximately 65° S (Schwerdtfeger, 1970). The presence of this belt is related to the baroclinity of the coastal atmosphere and extends up to at least the 500 hPa level. It is not continuous around the continent and its position shifts southward during the winter, when continental cooling intensifies. The migration of low-pressure cells drastically influences pressure patterns in the coastal zone and therefore the direction and strength of the geostrophic winds (Kottmeier, 1988; King, 1989; Heinemann and Rose, 1990).

4. Observed Mesoscale Atmospheric Structure

Surface observations and balloon soundings performed daily at Halley and GvN (Figure 2) enable us to track cyclones and anticyclones in the Weddell sea area. A high pressure area developed in the Weddell Sea in the last three weeks of January 1993. The area around GvN remained under the influence of an extended low pressure area. The mean wind vector and directional constancy at both coastal stations for the period 5 January to 10 February 1993 at standard pressure levels are given in Figure 3a. Winds at GvN were strong and persistent from the southeast throughout the lower troposphere, with high directional constancy that barely decreased with altitude. The turning of the wind with elevation suggests weak warm air advection between 925 and 850 hPa and cold air advection between 700 and 500 hPa. This implies that differential heat advection tends to destabilise the atmosphere at GvN. These measurements are in agreement with a thermal wind directed along the coast, promoting easterly winds in the boundary layer. A transition towards westerly winds can not be found under 500 hPa in the troposphere. This is probably a result of the weak upper air westerlies during the summer and the presence of the nearby semi-permanent cyclone centered at 65° S, 10° W (Kottmeier, 1988).

The mean winds at Halley were on average from the southwest but weak and variable throughout the lower troposphere (Figure 3a). Furthermore, balloon soundings show that the atmosphere up to 850 hPa was several degrees colder at Halley when compared to GvN (Figure 4). Apparently the circulation at Halley was strongly influenced by the high pressure build-up in the Weddell Sea, centered at 70° S, 40° W, during the last three weeks of January 1993. When considering the mean wind vectors of this period versus that of the remaining data (Figure 3b), we see that the mean flow at Halley was rather a superposition of two regimes: the lower panel broadly resembles the mean conditions at GvN as presented in Figure 3a and is associated with cyclonic activity that forces southeasterly winds

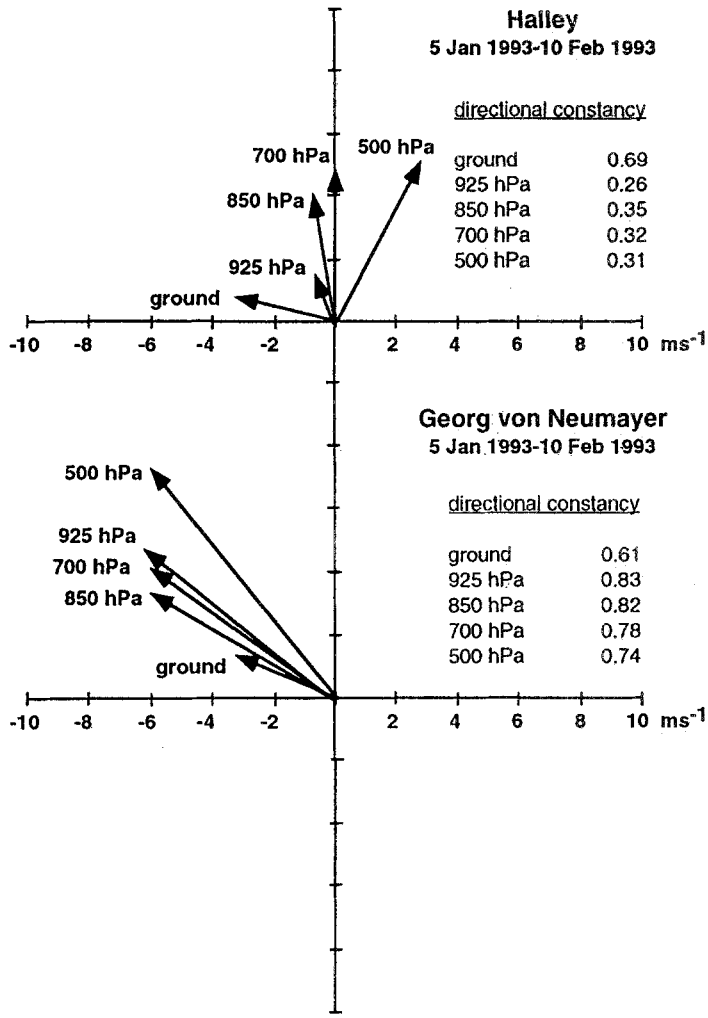

Fig. 3a. Mean wind vectors and directional constancy at standard pressure levels at Halley and Georg von Neumayer for the period 5 January–10 February 1993.

throughout the lower troposphere and a persistent downslope flow at the surface. The first panel, however, shows southwesterly flow at all levels except at the surface, where weak downslope flow persists. The latter flow type is associated with a high pressure ridge or a closed anticyclonic system in the Weddell sea. The thermal wind vector between 925 and 700 hPa indicates warm air advection at these levels while pronounced cold air advection is present between 700 and 500 hPa. This implies strong stabilisation of the lower troposphere at Halley.

The lower temperature below 850 hPa at Halley is a direct consequence of advection of cold air from the Ronne–Filchner ice shelf towards Halley during anticyclonic conditions in the Weddell Sea (King, 1989). To obtain an estimate

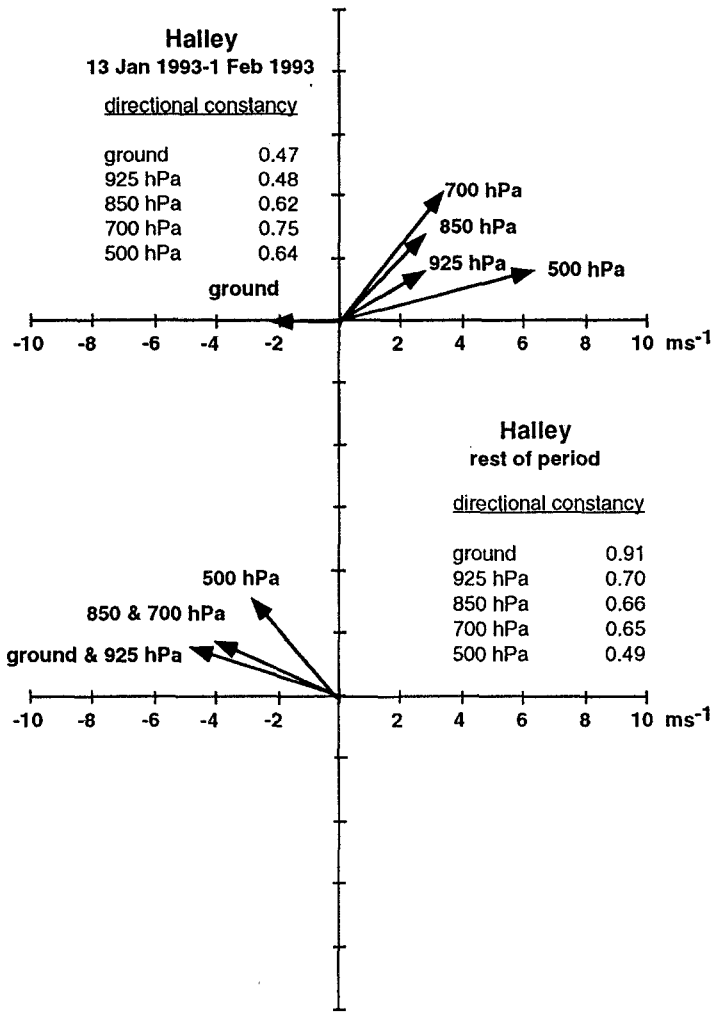

Fig. 3b. Same as Figure 3a, but for two different periods at Halley.

of the mesoscale temperature gradient between inland and coastal locations during these conditions, high resolution temperature soundings, performed at Halley during the period 14–19 January 1993, were compared with vertical temperature soundings at Svea during the same period (Figure 5). The result shows that the boundary layer between 850 and 770 hPa at Svea is warmer and less stable than the coastal environment at Halley, which is a surprising result. The usual meridional temperature contrast of the atmosphere between the ice sheet and surrounding seas has apparently reversed. The associated thermal wind parallel to the coast (Equation (1)) tends to produce west-east directed geostrophic winds in the boundary layer. This was observed at Svea on two consecutive days during this period. In general, however, geostrophic winds above the boundary layer are forced by synoptic pres-

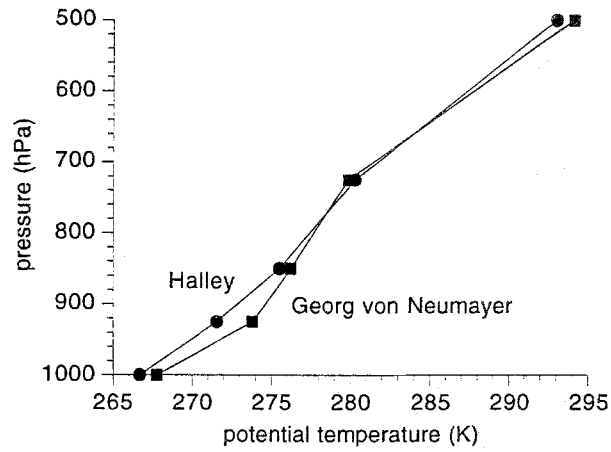

Fig. 4. Mean potential temperature at standard pressure levels at Halley and Georg von Neumayer for the period 5 January–10 February 1993.

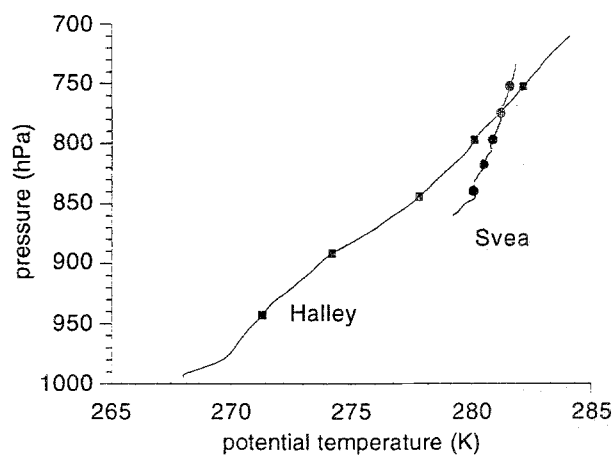

Fig. 5. Mean high resolution vertical profiles of potential temperature at Halley and Svea for the period 14–19 January 1993.

sure systems, and not by the mesoscale temperature gradient. This phenomenon can be attributed to the presence of the Riiser–Larsen ice shelf, reducing the thermal contrast between Svea and the coastal environment during the summer months. Moreover, high pressure areas that develop in the Weddell Sea initiate cold air advection to the coastal area. The Filchner–Ronne ice shelf, extending southwards to almost 85° S, provides an enormous basin of cold air for this mechanism.

Interesting differences can be noticed between the above-described situation and measurement performed by Kodama *et al.* (1989) at station D-47 in Adelie Land (67°23′ S, 138°43′ W). Upper air geostrophic winds at D-47 above 2500 m were persistent from westerly directions in contrast to northeasterly winds above

the boundary layer at Svea. This must be attributed to the time of their experiment (November–December) when the westerlies are still at their equinoctial maxima. In addition, the relatively northern position of D-47 (67° S) compared to Svea (74° S) makes it more sensitive to the westerly zonal circulation. Another significant difference is the observed thermal gradient in the atmosphere between the coastal zone and the inland ice. Kodama *et al.* (1989) measured a horizontal temperature gradient of 2.5 K 100 km^{-1}, whereas it was negligible and sometimes even reversed during our experiment (Figure 5). The process of cold air advection is not active in Adelie land, where the ice sheet ends directly in the sea. The low average value of wind speed during our experiment can be explained by the absence of strong thermal wind effects above the boundary layer, which is in contrast to measurements performed elsewhere on the continent.

5. Surface Wind in SBB

5.1. General meteorological conditions and flow types

The daily mean values of cloud cover, 6 m wind speed, 2 m temperature and 2 m relative humidity at Svea are presented in Figure 6. Days on which drifting snow was observed are marked with an 's'. Periods of one to several days with high wind speeds (from easterly directions) are characterised by advection of humid air to Svea, low atmospheric pressure and drifting snow. Precipitation was observed on several occasions, but could not be measured accurately. The time scale of several days indicates cyclonic activity at the coast. Weak local winds are associated with falling temperatures and less clouds, indicating the presence of a high pressure system in the Weddell Sea. Upper air wind direction was northeast on all days, except two. This indicates that the influence of the Weddell Sea anticyclone was not strong enough to force frequent southwesterly boundary-layer winds at Svea, as at Halley (King, 1989).

Wind direction frequency distributions at sites 2, 3, 4, 5 and 7 are presented in Figure 7. A clear trend can be observed. Outside the valley, easterly surface winds dominate; inside the valley, the wind direction has a bimodal distribution. Winds from the east are strong, while the second maximum (representing local slope flows) is associated with low wind speed. A criterium was developed to study both flow types individually, based on wind direction at Svea (site 7). All days with northeasterly winds >4 m s^{-1} were assigned to flow type I; days with southwesterly surface flow <4 ms^{-1} were assigned to flow type II. This criterium proved to be quite sharp, since all 42 days could be assigned to either type of flow: 23 to flow type I and 19 to flow type II. Mean characteristics of surface-layer parameters for both flow types are listed in Table III. During flow type I, strong easterly winds prevailed. Inside the valley, the mountains deflected the flow towards the southeast at site 2 and to the northeast at site 7, while the undisturbed wind direction at site 5 was from the east. A probable cause for the much lower wind speed at site 3 is divergence of the flow field, owing to the presence of a

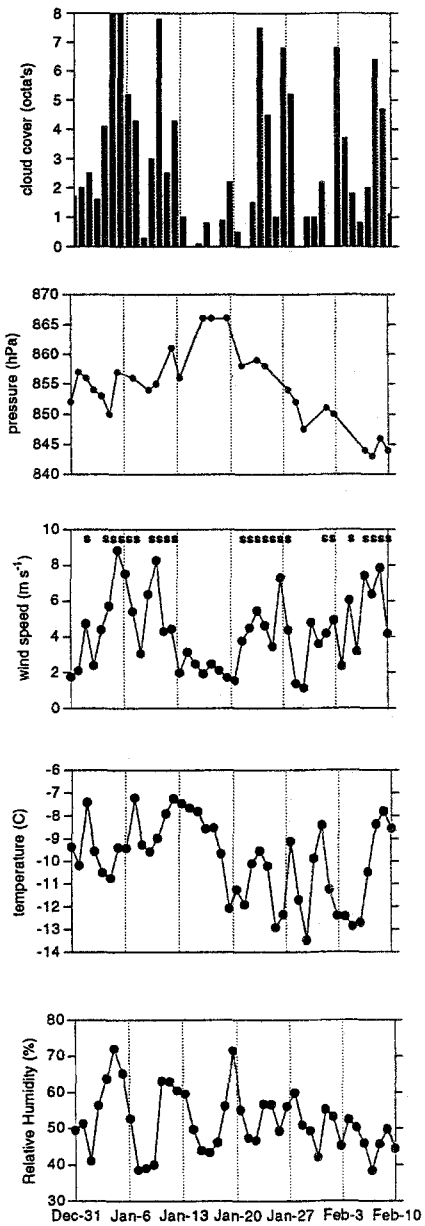

Fig. 6. Mean daily values of cloudiness, pressure, wind speed, temperature and relative humidity at Svea, for the period 31 December 1992–10 February 1993.

down-wind obstacle (Boyesennuten, Figure 2). Directional constancy was high everywhere for flow type I. The prevailing wind direction during flow type II was still east outside the valley, but became erratic inside the valley. Temperature inside

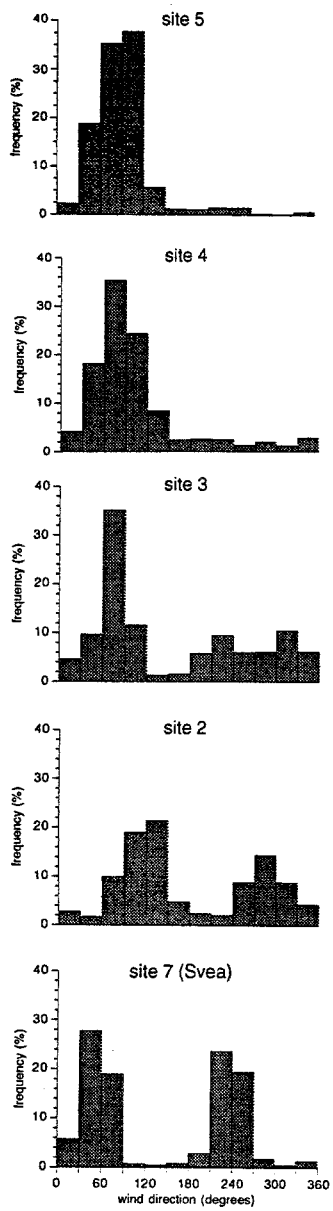

Fig. 7. Mean wind direction frequency distribution at sites 5, 4, 3, 2 and 7 (Svea) for the period 31 December 1992–10 February 1993.

the valley was 2–3 K higher than outside the valley for both flow types, probably owing to a föhn effect and lower albedo of the ice surface when compared to snow.

TABLE III

Flow and temperature characteristics for flow types I and II (see text)

Flow type	Site 2		Site 3		Site 4		Site 5		Site 7	
	1	2	1	2	1	2	1	2	1	2
Wind speed 6 m ($m\ s^{-1}$)	6.9	2.4	5.7	2.4	6.9	3.1	7.0	4.6	6.8	2.7
Friction velocity ($m\ s^{-1}$)	0.20	0.07	0.20	0.09	0.30	0.13	0.31	0.20	–	–
Wind dir. 6 m (deg.)	120	300	80	var.	80	80	80	80	60	150
Dir. const. 6 m	0.80	0.09	0.83	0.18	0.90	0.71	0.93	0.86	0.84	0.32
Temp. 2 m (°C)	−8.0	−9.3	−9.5	−10.4	−10.9	−11.1	−11.1	−12.1	−9.6	−10.3

5.2. Forcing of the surface layer outside the valley (site 4 and 5)

In Figure 8, the mean daily cycle for the entire period of wind speed (6 m), temperature (2 and 6 m), gradient Richardson number Ri_g and net radiation (1 m) at site 5 are presented. The gradient Richardson number is defined as:

$$Ri_g = \frac{g\Delta\overline{\theta_v}\Delta z}{\overline{\theta_v}[(\Delta\overline{u})^2 + (\Delta\overline{v})^2]}, \tag{2}$$

where the differences in temperature and wind speed are measured between 2 and 6 m. The strong radiative cooling of the surface results in a larger temperature inversion at night associated with a katabatic wind that has a pronounced downslope component, resulting in the maximum surface wind speed at 04 UT. During the day, most of the solar radiation is reflected at the surface, which has an albedo of 0.80. The rest is absorbed in the top few centimeters of the snow layer. At 10 UT, the stratification of the surface layer between 2 and 6 m becomes unstable (negative Ri_g). As a result, vertical mixing occurs throughout the surface layer and the katabatic force vanishes. The surface flow veers toward the upper air geostrophic wind direction, which had a predominant cross-slope component, associated with the prevailing synoptic pressure distribution during the experiment. This situation is reversed at 19 UT, when the surface layer quickly develops towards stable stratification (large positive Ri_g) in response to the negative radiation budget. This daily cycle of the wind direction is a very consistent feature, given the high values of the directional constancy throughout the day. Broad similarities in thermal stratification of the surface layer can be found between site 5 and those reported by Wendler (1988) at D-47 at the other side of the continent.

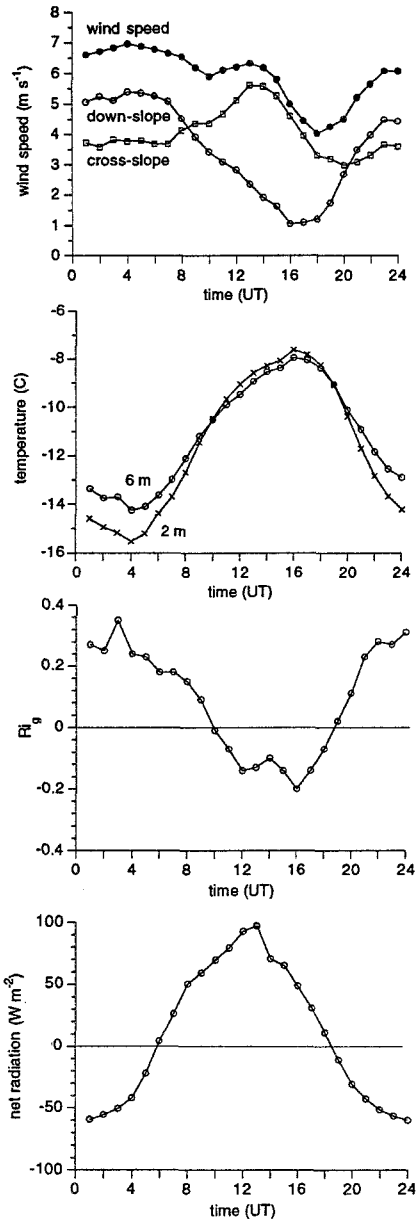

Fig. 8. Mean daily cycle at site 5 of wind speed (cross-slope and downslope component), temperature, gradient Richardson number Ri_g and net radiation (taken from site 3) for the period 31 December 1992–10 February 1993.

5.3. FORCING OF THE SURFACE LAYER INSIDE THE VALLEY (SITE 2, 3 AND 7)

The presence of slopes with different orientation inside the valley apparently has large implications for the flow regime. Even when no clear trend could be detected

in the upper air flow, surface wind direction inside the valley showed large variation. Following the theoretical approach of Kottmeier (1986), we study the influence of surface slope vector and upper air geostrophic wind vector on surface wind direction, as a function of surface layer stability. We define the x-axis to point down the local slope (Figure 9). The upper air geostrophic wind vector is denoted by $\mathbf{V}_h$ (where h stands for the height of the Ekman layer) and the surface wind vector is given by $\mathbf{V}_s$. The angle between $\mathbf{V}_h$ and the downslope direction is γ, the angle between $\mathbf{V}_s$ and downslope direction is δ, so the angle between $\mathbf{V}_h$ and $\mathbf{V}_s$ equals γ–δ. Assuming stationarity and horizontal homogeneity (no thermal wind effects inside the boundary layer), we can write the simplified equations of motion as:

$$fv - fv_h = \frac{\partial(\overline{w'u'})}{\partial z} - g\frac{\Delta\theta}{\theta_0}\sin(\alpha), \tag{3}$$

$$-fu + fu_h = \frac{\partial(\overline{w'v'})}{\partial z}, \tag{4}$$

where u represents downslope motion, v cross-slope motion, w vertical motion, f the Coriolis parameter, $\Delta\theta$ the surface inversion strength and α the surface slope angle. The second term on the right hand side in (3) represents the horizontal pressure gradient induced by an inversion present over a sloping surface (katabatic force). $\Delta\theta$ is the height-dependent temperature difference between the inversion layer and the free atmosphere, where θ_0 is the undisturbed background value. The geostrophic wind components u_h and v_h are given by the synoptic pressure gradients above the inversion layer, $(1/\rho_0\ \partial p/\partial y)_h$ and $(1/\rho_0\ \partial p/\partial x)_h$, respectively. Surface friction is assumed to follow a quadratic drag law:

$$(\overline{w'u'})_0 = -C_d(u_s^2 + v_s^2)\cos(\delta) \qquad (\overline{w'v'})_0 = -C_d(u_s^2 + v_s^2)\sin(\delta), \tag{5}$$

where C_d is the drag coefficient for momentum, in our case referring to a height of 6 m, which also holds for the surface components of the wind vector u_s and v_s. To keep interpretation straightforward, we assume a stability-independent value for C_d of 0.002. In order to estimate the vertical divergence of momentum flux, the boundary-layer depth h is estimated as (Arya, 1981):

$$h = a_1\frac{\kappa u_*}{|f|}, \tag{6}$$

where κ is the von Kármán constant while the constant $a_1 < 1$ is included to account for the fact that this expression was developed for neutral coditions, while conditions in Antarctica are generally stable. Integrating the stress terms from the surface to h, we get

$$\frac{\partial(\overline{w'u'})}{\partial z} = \frac{a_2\sqrt{C_d}|f|u_s}{a_1\kappa} \qquad \frac{\partial(\overline{w'v'})}{\partial z} = \frac{a_2\sqrt{C_d}|f|v_s}{a_1\kappa}, \tag{7}$$

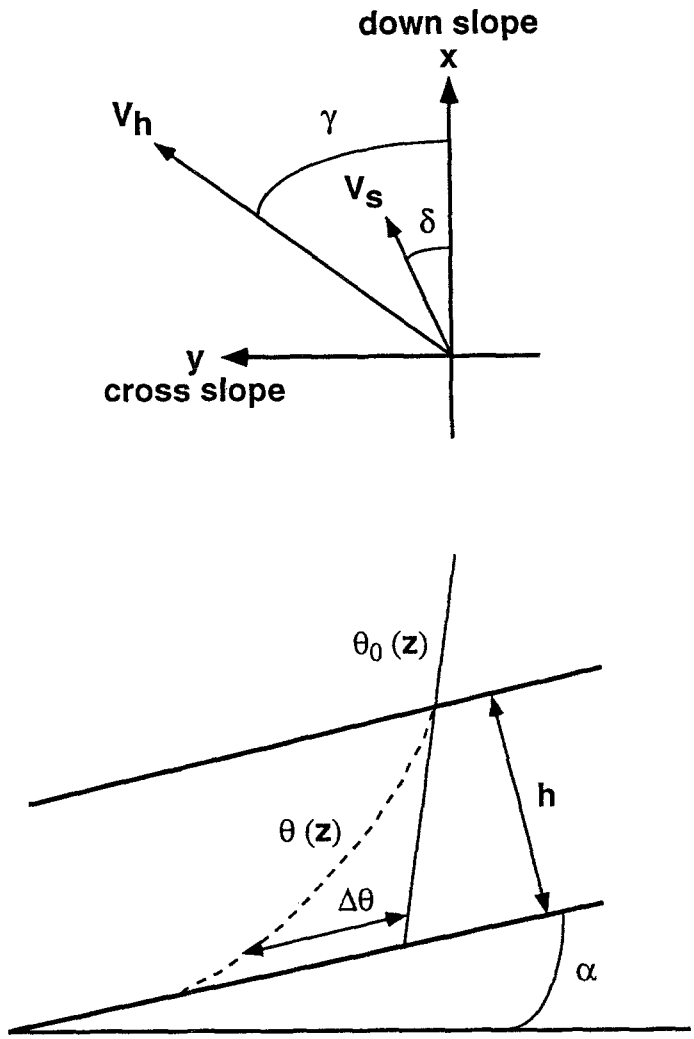

Fig. 9. Orientation of axes and meaning of symbols according to Kottmeier (1986).

where the constant a_2 accounts for the varying stress gradients along the profile. It is clear from (3) and (4) that using a single value of a_2 is not justified theoretically. Computations with varying a_2 showed that the surface wind direction was much more sensitive to $\Delta\theta$ than to a_2. For the present study, the assumption of a constant factor $a = a_2/a_1$, following Kottmeier, seems justified. However, this asumption restricts us to computation of surface wind direction only, since for wind speed, the asymmetry factors will certainly be important. Upon substituting (7) into (3) and (4) and solving for δ, we obtain:

$$\tan(\delta) = \frac{v_6}{u_6} = \frac{1 - \zeta_1\zeta_2}{\zeta_1 + \zeta_2}, \tag{8}$$

where

$$\zeta_1 = \frac{u_h}{v_h - \frac{g\Delta\theta}{|f|\theta_0}\sin(\alpha)} \quad \text{and} \quad \zeta_2 = \frac{a\sqrt{C_d}}{\kappa}. \tag{9}$$

Equations (8) and (9) state that for very stable cases $\delta < 90°$, i.e., the surface flow can only have a downslope component. This also holds for a cross-slope directed geostrophic wind ($\zeta_1 = 0$). From the definition of ζ_1, we see that only the cross-slope component of the surface flow is affected by the local forcing, while ζ_2 represents friction effects. This theory is not suitable to predict absolute wind directions at the surface, since local slope directions and magnitudes are hard to verify. Moreover, inclusion of Coriolis forcing in (3) and (4) excludes study of pure downslope flows, which are known to occur frequently during the short Antarctic summer nights. However, it is a convenient tool to study the strong variations in wind direction inside SBB.

For a north-south directed geostrophic flow above the boundary layer, a typical value for γ outside the valley is 135° with a slope $\sin(\alpha) = 17$ m km^{-1}. Representative for inside the valley, we choose $\gamma = 265°$ and $\sin(\alpha) = 34$ m km^{-1}. The results of applying (8) to both locations are presented in Figures 10a and b, where for convenience γ–δ is plotted instead of δ and we use $G = |V_h|$. Flow type I is associated with geostrophic wind speed $G > 10$ m s^{-1} and near neutral stratification throughout the day (clouds, strong mixing). In both Figures 10a and b this corresponds to a small daily variation of δ and an angle between geostrophic wind above the boundary layer and surface wind (equal to γ–δ) which is comparable at both sites. Flow type II, however, is characterised by small G and a large daily variation in inversion strength (clear sky, small wind speeds). Figure 10a suggests for this case that the daily variation of δ outside the valley will increase but that the change in mean surface wind direction will be small. Flow inside the valley under these conditions becomes very sensitive for complete rotation of 180° (Figure 10b), depending on the exact value of G and the inversion strength. If for instance $G = 10$ m s^{-1}, the surface flow will turn to a downslope direction (opposite to G) whenever the inversion strength exceeds only 1 K. This will frequently be the case, stressing the persistence of the local circulation.

The observed average daily cycles of wind direction at sites 3 (inside the valley), 4 and 5 (outside the valley) are given in Figure 11 for both flow types. Wind direction for flow type I shows small diurnal variation and has the same direction at all sites, which is in agreement with the theory. During flow type II the daily variation of wind direction at sites 4 and 5 has increased, but mean wind direction has not changed. Inside the valley, however, on average we observed a reversal in wind direction for flow type II from west to east, also in agreement with theory (Figure 10b). The exact time of this reversal was not constant throughout the experiment, though, and sometimes the reversal did not occur at all. This can be understood from Figure 10b: on days with small G, the surface temperature

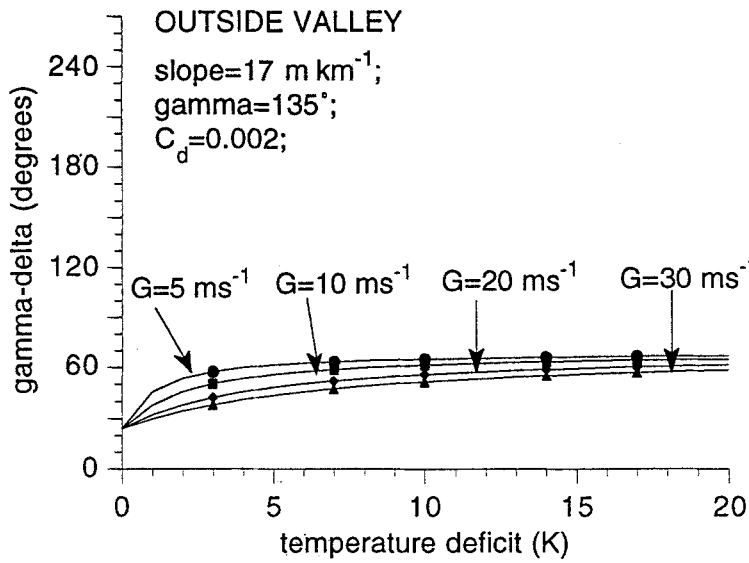

Fig. 10a. Angle between upper air geostrophic vector and 6 m 'surface' wind direction according to Equation (8). Parameter values represent typical conditions out of the valley (site 5).

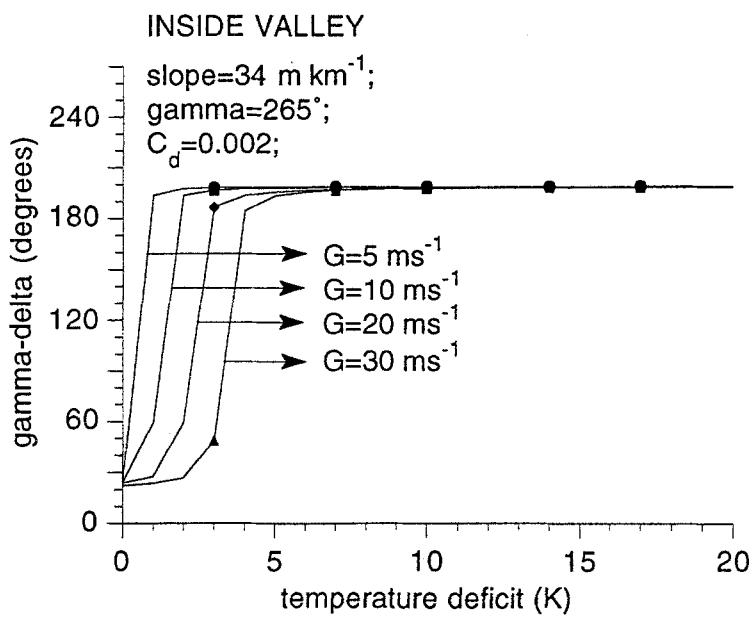

Fig. 10b. As in Figure 10a but for typical in-valley parameter values (site 2).

inversion must decrease to zero (lapse conditions) in order to establish reversal of the flow towards upslope direction (large γ–δ). Apparently surface cooling on these days was strong enough to maintain a surface inversion, resulting in persistent westerly surface flow.

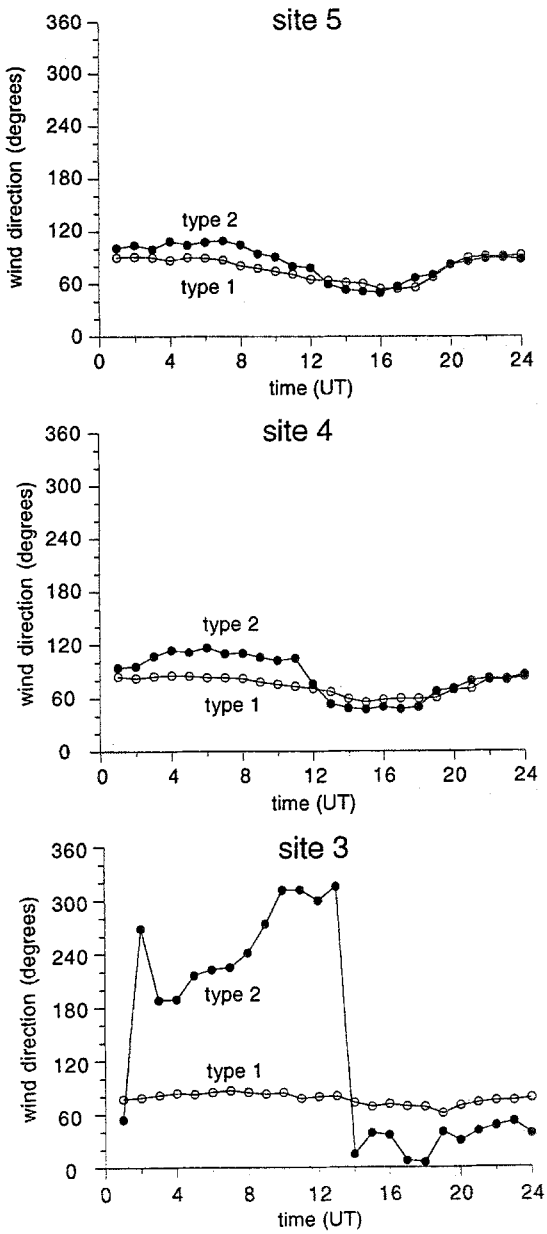

Fig. 11. Mean daily cycle for 6 m wind direction at sites 5, 4 and 3, for both flow types.

The detailed structure of the boundary layer inside the valley during flow type II was investigated using a cabled balloon at site 7. A period of 6 days was selected (14–19 January 1993) during which flow type II dominated. Reversal of the surface wind inside the valley occurred on 3 of the 6 days in this period. Mean time-height cross-sections of potential temperature, specific humidity, wind speed

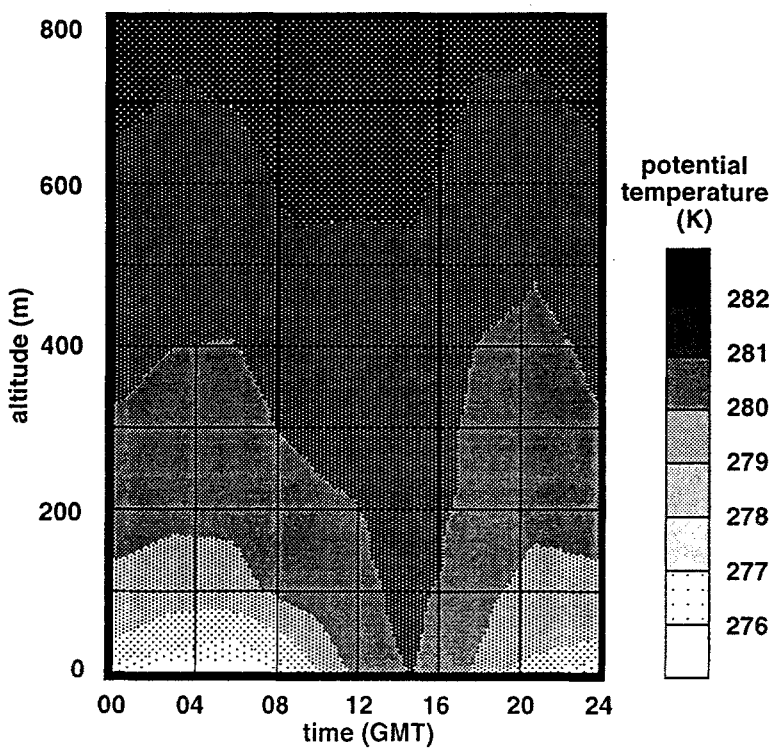

Fig. 12a. Mean time height cross-section of potential temperature at Svea, 14–19 January 1993.

and directional constancy averaged over this period are presented in Figures 12a–d. If we assume the situation at 800 m to represent free atmosphere conditions, the inversion strength is typically 7 K at 06 UT and less than 1 K at 15 UT (Figure 12a). According to Figure 10b this is sufficient to establish a 180° rotation of the 6 m wind at 15 UT, which actually happens at exactly that time (Figure 12c).

Dark areas in Figure 12d represent persistent flow features that occur every day during the 6-day period under consideration (high directional constancy). A shallow downslope flow develops during the short night and reaches a maximum depth of 40 m at 10 UT. This shallow flow is driven by negative buoyancy and retarded by friction and advection of weaker momentum (Mahrt, 1982). The elevated area with high directional constancy represents the geostrophic flow (from the northeast) above the boundary layer. The area of very small directional constancy throughout the boundary layer around 10 UT represents the time band in which the upper air flow starts to penetrate towards the surface, in response to heating of the boundary layer and hence decreased stability. Since this does not happen at the same time every day, there must be a time interval during which on average, the vector mean wind speed is low, producing low values of directional constancy. Analogously, low directional constancy at the surface in the afternoon indicates that the surface is not reached every day by the upper air flow. A significant feature

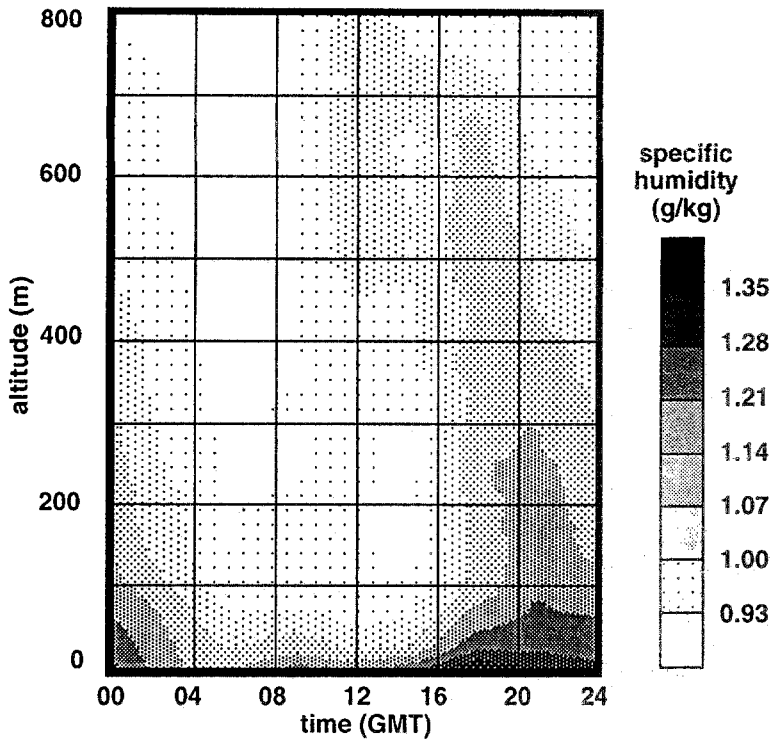

Fig. 12b. Same as Figure 12a, but for specific humidity.

is the frontal zone that shows up throughout the whole boundary layer in Figure 12d, indicating that entrainment of upper air flow happens every day at the time that local stratification becomes neutral. The present analysis suggested that especially during the Antarctic winter, when longwave radiative cooling dominates the surface energy balance, upper air winds can hardly penetrate towards the surface inside the valley. Existence of a persistent circulation inside the valley during winter has been confirmed by Jonsson (1992). The influence of the type of circulation on the moisture budget of the boundary layer is illustrated in Figure 12b. Specific humidity content in the surface layer is severely reduced (and evaporation at the surface enhanced) whenever mixing with the upper atmosphere occurs. Stabilising of the surface layer after 15 UT results in decoupling of the surface flow from the upper air flow, suppressing evaporation from the surface. That means that evaporation will be reduced during flow type II and enhanced during flow type I.

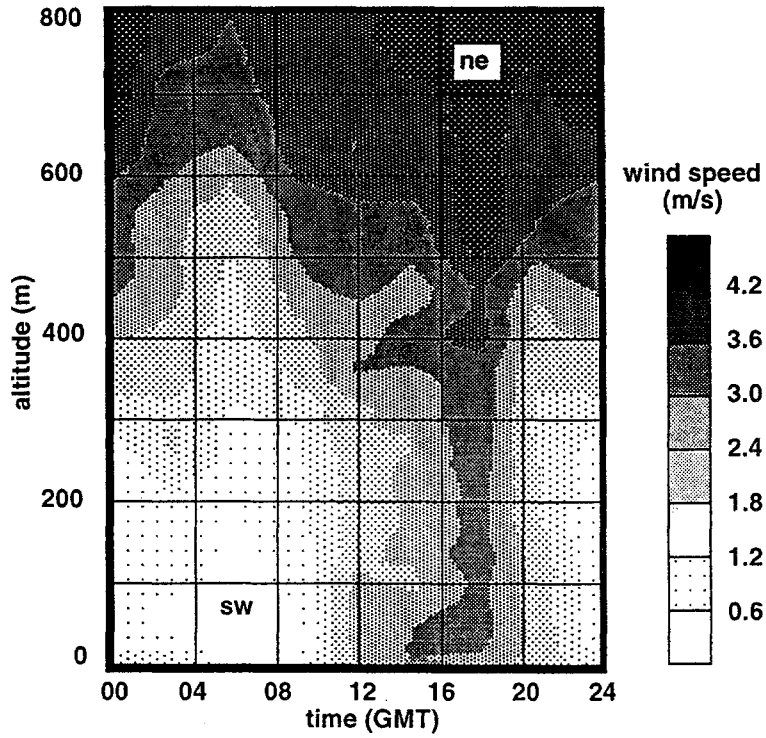

Fig. 12c. Same as Figure 12a, but for absolute wind speed.

6. Implications for the Energy and Mass Balance

Providing that no melt occurs, the surface energy balance of snow and ice can be expressed as:

$$Shw + Lw + H + LE + G = 0, \tag{10}$$

where Shw represents the net shortwave radiation flux, Lw the net longwave radiation flux, H the sensible heat flux, LE the latent heat flux and G the sub-surface heat flux. A detailed study of the surface energy balance of snow and blue ice is presented by Bintanja and Van den Broeke (in press). The average magnitude of the different terms is presented in Figure 13, for site 2 (blue ice) and site 5 (snow) and for the two flow types (positive net energy flux is directed towards the surface). Owing to the relatively low albedo of blue ice (0.56), the net shortwave flux is larger at site 2 than at site 5 (average albedo 0.80). This extra energy is almost completely lost by the longwave radiation balance: the blue ice surface is warmer and therefore loses more energy through longwave radiation. All other terms over the blue ice represent energy losses. At site 5 on the other hand, the sensible heat flux is directed towards the surface. Consequently, the air is cooled in the lower layers and stratification will be more stable than over blue ice.

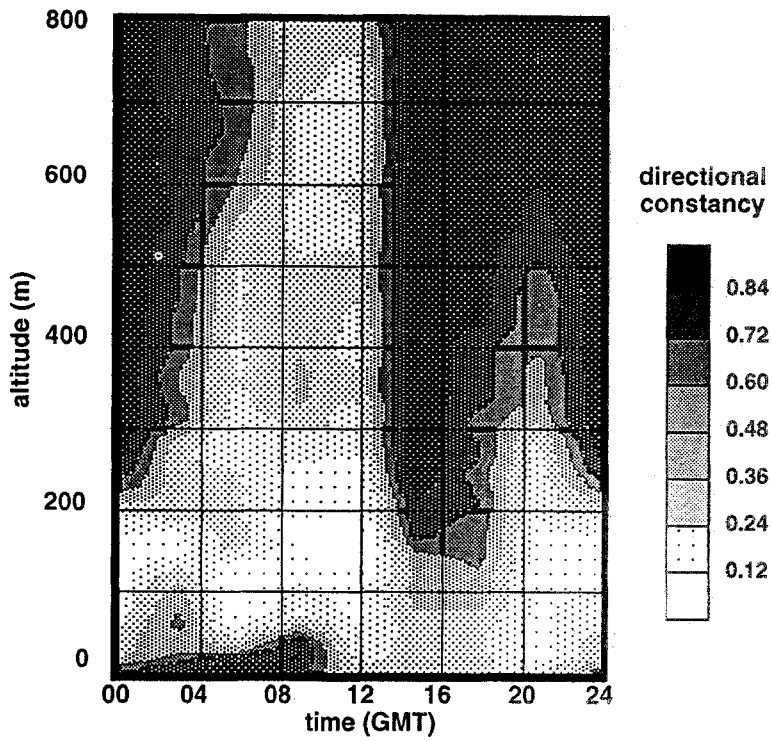

Fig. 12d. Same as Figure 12a, but for directional constancy.

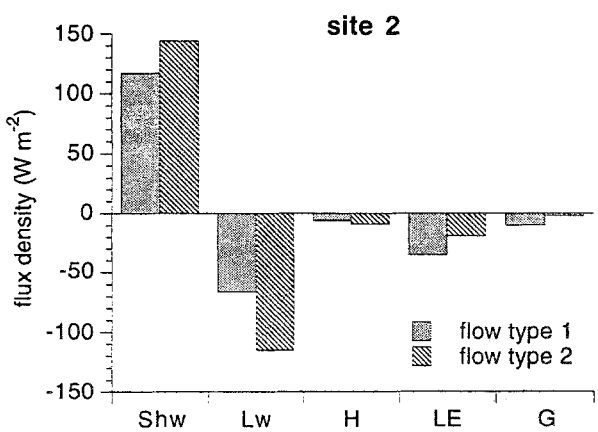

Fig. 13a. Surface energy balance terms at site 2, for both flow types. Shw: net shortwave radiation; Lw: net longwave radiation; H: sensible heat flux; LE latent heat flux; G sub-surface heat flux.

Comparing surface energy balance characteristics for the different flow types, we see that high cloud cover during flow type I forces the net longwave radiation to be less negative. At site 5, the difference even overcompensates the decreased

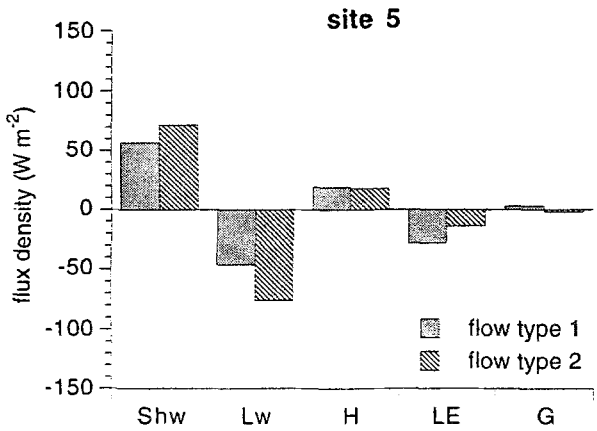

Fig. 13b. As Figure 13a, but for site 5.

incoming shortwave radiation flux. This phenomenon is commonly referred to as the radiation paradox. Sublimation, important for the mass balance of the blue ice area, is a significant term in the energy balance only during flow type I (35 W m^{-1} over the blue ice, corresponding to 1 mm w.e. per day). Note that at site 5 the flux of latent heat is only 10 W m^{-2} smaller than over the blue ice, although the amount of solar energy available is much smaller. This can be attributed to the larger average wind speed at site 5 and the rougher surface (Tables II, III), both factors promoting evaporation. The sublimation gradient between site 5 and 2 will thus not be very steep.

Both evaporation and divergence of drifting snow are important for maintaining the local mass balance gradient of BIA's. When a local circulation develops, mixing with upper air is generally poor. In spite of the combination with clear weather, this leads to the conclusion that the local circulation decreases evaporation and serves as a negative feedback for the maintenance of the mass balance gradient. It is argued that, on the otherhand, *formation* of BIA's will not be hindered by this negative feedback process. Conditions favourable for BIA formation (the divergence of large amounts of drifting snow) occur when wind speed exceeds 8–10 m s^{-1} at the surface, i.e., if the flow type I prevails. The present observations support the idea that BIA's are mainly created by enhanced divergence of drifting snow, and not by spatial variation of sublimation, although the latter can be significant during summer. In winter, evaporation is generally very small, or even changes to condensation.

7. Conclusions

Forcing of the surface wind over the BIA under consideration is determined by stabilising/destabilising of the surface layer and the strength of the upper air geostrophic flow. A theoretical model developed by Kottmeier (1986) is well able to repro-

duce the thresholds for formation/removal of the local circulation inside the valley. A surprising results is that the thermal contrast between Svea and the coast (300 km to the North) is small. Thus, the geostrophic flow above the boundary layer is mainly forced by the synoptic pressure gradient, and not by thermal wind effects. On average, the observed surface wind speed is much smaller than that observed elsewhere on the continent at a similar elevation. Two factors are responsible: owing to strong mixing in the daytime the katabatic forcing disappears. Moreover, no strong thermally-forced winds are present above the boundary layer in this part of Antarctica: the presence of the Larsen ice shelf tends to decrease the temperature gradient between SBB and the coast, especially when cold air is being advected from the Filchner–Ronne ice shelf. This mesoscale atmospheric structure differs significantly from that observed in Adélie Land by Kodama *et al.* (1989), where strong thermal winds trade places with katabatic forcing in the daytime.

The measurements presented in this paper are probably representative for BIA's: the persistent valley circulation is a year-round feature, as observed by Jonsson (1992), while the average synoptic situation at Halley very well resembles the 1985 wind climatology during summer, as presented by King (1989). The local circulation, induced by the presence of a depression in the topography, acts as a negative feedback for maintaining the mass balance gradient because of decreased evaporation of the ice surface. However, during conditions that are favourable for BIA formation (strong upper air and surface winds), a local circulation will probably not develop.

Acknowledgements

We would like to thank the participants of 92–93 Nordic Antarctic Research Program for the logistical support during the expedition. Marcel Portanger is thanked for technical support and Louk Conrads for logistical support in Utrecht. Hans Oerlemans, Stig Jonsson and Peter Duynkerke gave valuable comments on the manuscript. Important thanks go to John King from the British Antarctic Survey, who provided us with the synoptic maps of the Wedell sea area (from the Met. Office in Bracknell) and surface observations as well as vertical soundings performed at Halley and Georg von Neumayer. Funding for this project was provided by the Dutch National Research Programme on Global Air Pollution and Climate Change (NOP) and the Netherlands Marine Research Foundation (SOZ).

References

Arya, S. P. S.: 1981, 'Parameterizing the Height of the Stable Atmospheric Boundary Layer', *J. Appl. Meteorol.* **20**, 1192–1202.

Ball, K. F.: 1956, 'The Theory of Strong Katabatic Winds', *Aust. J. Phys.* **9**, 373–386.

Bintanja, R., van den Broeke, M. R., and Portanger, M. P.: 1993, 'A Meteorological and Glaciological Experiment on a Blue Ice Area in the Heimefront Range, Queen Maud Land', Antarctica, Svea Field Report, Utrecht University.

Bintanja, R. and van den Broeke, M. R.: 1994, 'The Surface Energy Balance of Antarctic Blue Ice and Snow', *J. Appl. Meteorol.* in press.

Bromwich, D. H.: 1989, 'Satellite Analysis of Antarctic Katabatic Wind Behaviour', *Bull. Am. Meteorol. Soc.* **70**, 738–749.

Cassidy, W., Harvey, R., Schutt, J., Delisle, G., and Yanai, K.: 1992, 'The Meteorite Collection Sites of Antarctica', *Meteoritics* **27**, 490–525.

Clow, G. D., McKay, C. P., Simmons Jr., G. M., and Wharton Jr., R. A.: 1988, 'Climatological Observations and Predicted Sublimation Rates at Lake Hoare, Antarctica', *J. Climate* **1**, 715–728.

Fortuin, J. P. F. and Oerlemans, J.: 1990, 'Parametrization of the Annual Surface Temperature and Mass Balance of Antarctica', *Ann. Glac.* **14**, 78–84.

Fujii, Y. and Kusunoki, K.: 1982, 'The Role of Sublimation and Condensation in the Formation of Ice Sheet Surface at Mizuho Station, Antarctica', *J. Geophys. Res.* **87**(C6), 4293–4300.

Heinemann, G. and Rose, L.: 1990, 'Surface Energy Balance, Parametrizations of Boundary-Layer Heights and the Application of Resistance Laws Near an Antarctic Ice Shelf Front', *Boundary-Layer Meteorol.* **51**, 123–158.

Jonsson, S.: 1992, 'Local Climate and Mass Balance of an Antarctic Blue-Ice Area', *Zeitschrift für Gletscherkunde und Glazialgeologie* **27**, 11–29.

King, J. C.: 1989, 'Low-Level Wind Profiles at an Antarctic Coastal Station', *Antarctic Science* **1**(2), 169–178.

Kodama, Y., Wendler, G., and Ishikawa, N.: 1989, 'The Diurnal Variation of the Boundary Layer in Summer in Adélie Land, Eastern Antarctica', *J. Appl. Meteorol.* **28**, 16–24.

Kottmeier, C.: 1986, 'The Influence of Baroclinity and Stability on the Wind and Temperature Conditions at the Georg von Neumayer Antarctic Station', *Tellus* **38A**, 266–276.

Kottmeier, C.: 1988, 'Atmosphärische Strömungsvorgaange am Rande der Antarktis', *Berichte des Institutes für Meteorologie und Klimatologie der Universität Hannover*, Band 33.

Kottmeier, C. and Stuckenberg, H.: 1986, 'A Quasi Geostrophic Flow Solution for the Circulation over Antarctica', *Beitr. Phys. Atmosph.* **59**(4), 491–503.

Mahrt, L. J. and Schwerdtfeger, W.: 1970, 'Ekman Spirals for Exponential Thermal Wind', *Boundary-Layer Meteorol*, **1**, 137–145.

Mahrt, L.: 1982, 'Momentum Balance of Gravity Flow', *J. Atmos. Sci.* **39**, 2701–2711.

McKendry, I. G. and Lewthwaite, E. W. D.: 1989, 'The Vertical Structure of Summertime Local Winds in the Wright Valley, Antarctica *Boundary-Layer Meteorol.* **51**, 321–342.

Oerlemans, J. and Vugts, H. F.: 1993, 'A Meteorological Experiment in the Melting Zone of the Greenland Ice Sheet', *Bull. Am. Meteorol. Soc.* **74**(3), 355–365.

Ohata, T., Kobayashi, S., Ishikawa, N., and Kawaguchi, S.: 1985, 'Structure of the Katabatic Winds at Mizuho Station, East Antarctica', *J. Geophys. Res.* **90**, 10651–10658.

Orheim, O. and Lucchitta, B.: 1990, 'Investigating Climate Change by Digital Analysis of Blue Ice Extent on Satellite Images of Antarctica', *Annals of Glaciology* **14**, 211–215.

Parish, T. R.: 1984, 'A Numerical Study of Strong Katabatic Winds over Antarctica', *Mon. Wea. Rev.* **112**, 545–554.

Parish, T. R. and Waight, K. T.: 1987, 'The Forcing of Antarctic Katabatic Winds', *Mon. Wea. Rev.* **115**, 2214–2226.

Parish, T. R. and Bromwich, D. H.: 1991, 'Continental-Scale Simulation of the Antarctic Katabatic Wind Regime', *J. Climate* **4**, 135–146.

Pettré, P. and André, J. C.: 1991, 'Surface Pressure Change Through Loewe's Phenomena and Katabatic Flow Jumps: Study of Two Cases in Adélie Land, Antarctica', *J. Atmos. Sci.* **48**(4), 557–571.

Schwerdtfeger, W.: 1970, 'Weather and Climate of the Antarctic, Ch. 4, Volume XIV', in S. Orvig, (ed.), *World Survey of Climatology*, Elsevier, New York, pp. 253–355.

Sorbjan, Z., Kodama, Y., and Wendler, G.: 1986, 'Observational Study of the Atmospheric Boundary Layer over Antarctica', *J. Climate Appl. Meteorol.* **25**, 641–651.

Takahashi, S., Naruse, R., Nakawo, M., and Mae, S.: 1988, 'A Bare Ice Field in East Queen Maud Land, Antarctica, Caused by Horizontal Divergence of Drifting Snow', *Annals of Glaciology* **11**, 156–160.

Van den Broeke, M. R. and Bintanja, R.: 1994, 'On the Interaction of Katabatic Winds and Blue Ice Area Formation in East Antarctica', *Journal of Glaciology*, in press.
Wendler, G. and Kodama, Y.: 1985, 'Some Results of Climatic Investigations of Adélie Land, Eastern Antarctica', *Zeischrift für Gletscherkunde und Glazialgeologie* **21**, 319–3217.
Wendler, G., Ishikawa, N., and Kodama, Y.: 1988, 'The Heat Balance of the Icy Slope of Adélie Land, Eastern Antarctica', *J. Appl. Meteorol.* **27**, 52–65.